Journal of Systems Engineering and Electronics
Vol. 32, No. 3, June 2021, pp.573 – 583

Adaptive digital self-interference cancellation based on fractional order LMS in LFMCW radar

LUO Yongjiang*, BI Luhao, and ZHAO Dong

School of Electronic Engineering, Xidian University, Xi'an 710071, China

Abstract: Adaptive digital self-interference cancellation (ADSIC) is a significant method to suppress self-interference and improve the performance of the linear frequency modulated continuous wave (LFMCW) radar. Due to efficient implementation structure, the conventional method based on least mean square (LMS) is widely used, but its performance is not sufficient for LFMCW radar. To achieve a better self-interference cancellation (SIC) result and more optimal radar performance, we present an ADSIC method based on fractional order LMS (FOLMS), which utilizes the multi-path cancellation structure and adaptively updates the weight coefficients of the cancellation system. First, we derive the iterative expression of the weight coefficients by using the fractional order derivative and short-term memory principle. Then, to solve the problem that it is difficult to select the parameters of the proposed method due to the non-stationary characteristics of radar transmitted signals, we construct the performance evaluation model of LFMCW radar, and analyze the relationship between the mean square deviation and the parameters of FOLMS. Finally, the theoretical analysis and simulation results show that the proposed method has a better SIC performance than the conventional methods.

Keywords: adaptive digital self-interference cancellation (ADSIC), linear frequency modulated continuous wave (LFMCW) radar, fractional order least mean square (LMS).

DOI: 10.23919/JSEE.2021.000049

1. Introduction

Linear frequency modulation continuous wave (LFMCW) radar has the advantages of no blind spots, high receiver sensitivity, high range resolution, and small size. It is widely used in navigation radar [1], automotive radar [2−4] and other fields. However, the existence of self-interference (SI) seriously reduces the isolation between the transmitter and the receiver in LFMCW radar. Therefore, in order to achieve higher isolation, the self-interference cancellation (SIC) technology is particularly critical.

According to the SIC implementation location, the SIC is classified into three categories: space SIC (SSIC), analog SIC (ASIC) and digital SIC (DSIC). SSIC suppresses the SI signal power by using the antenna natural isolation, antenna directivity, antenna polarization and so on [5−8]. ASIC is placed at the front end of the receiver channel to limit the power of SI signals to the dynamic range of the analog to digital converter (ADC) [9−13]. In [14], an improved isolation method based on convex optimization was proposed, which suppressed the signal coupled to the receiver by the zero-point technique. In [15], an X-band cancellation test system based on digital cancellation technology was developed for LFMCM radar. However, the above implementation ASIC methods are not flexible and analog circuit is too complicated. Thus, the DSIC method is widely used because of its advantages such as easy implementation, low complexity, and high calculation accuracy [16,17].

To adaptively track the change of signal channels and signal characters, more and more researchers pay attention to the adaptive DSIC (ADSIC) method. With advantages of its simple structure, stable performance and easy implementation, least mean square (LMS) has been utilized in ADSIC [18]. The LMS-based ADSIC method uses the digital baseband signal as the reference signal to produce the cancellation signal, which is subtracted from the received signal to suppress the SI signals. In [19], the initial delay and frequency offset were compensated by the LMS-based ADSIC method, which tracked the changes of the SI signal amplitude and phase to produce the cancellation signal. Finally, it eliminated SI signals by approximately 20 dB. In [20,21], an ADSIC method based on the recursive least square (RLS) algorithm was proposed. Compared to the ADSIC method based on LMS, its convergence time is shorter, but the implementation is complex. The ADSIC method based on LMS and RLS are widely used in the communication field based on the stationary signal.

Manuscript received July 22, 2020.
*Corresponding author.

The LMS-based ADSIC method is implemented by the integer order gradient descent (IOGD) and the cancellation performance of the ADSIC method could be improved. However, the emergence of fractional order gradient descent (FOGD) method brings possibility to obtain a better performance. In [22], by using the Caputo's fractional derivative theory, the author proposes the fractional order LMS (FOLMS). It is pointed out that the larger the fractional gradient order, the greater the weight noise, and the smaller the fractional gradient order, the smaller the weight noise and the slower the convergence rate. Specifically, when the fractional gradient order is greater than 1, its convergence rate is faster than the LMS, when the fractional gradient order is smaller than 1, it also brings small steady-state error. In [23,24], the FOLMS consisting of IOGD and FOGD was proposed. It is mentioned that when the fractional gradient order increases to 1, the convergence rate and steady-state error will increase.

In order to achieve higher SI suppressing and improve the isolation, an ADSIC method based on the FOLMS in LFMCW radar is proposed. First, we modify the conventional ADSIC method by fractional order gradient which is calculated by Caputo's derivative. Then, to solve the problem that the long memory characteristic of fractional order derivative leads to the non-convergence of the algorithm, we utilize the short-term memory principle to ensure the convergence of the proposed algorithm. Furthermore, from the nonstationary and time-varying perspective, we analyze the influence of the fractional order and the step size on the mean square deviation of the proposed algorithm in the steady state, which provides a theoretical basis for the practical application of the algorithm. Finally, the performance and superiority of the proposed method are shown by using simulation and experimental data.

The rest of this paper is organized as follows. Section 2 introduces the ASIC and the ADSIC system model of LFMCW radar in detail, and Section 3 presents the ADSIC method based on FOLMS. In Section 4, simulation results of the different cases are provided to illustrate the efficiency and superiority of the proposed method. Conclusions are given in Section 5.

2. System model

In this section, the simplified system model of LFMCW radar is described in detail. Fig. 1 shows the block diagram for the proposed ADSIC method, where the analog domain and the digital domain SIC are included.

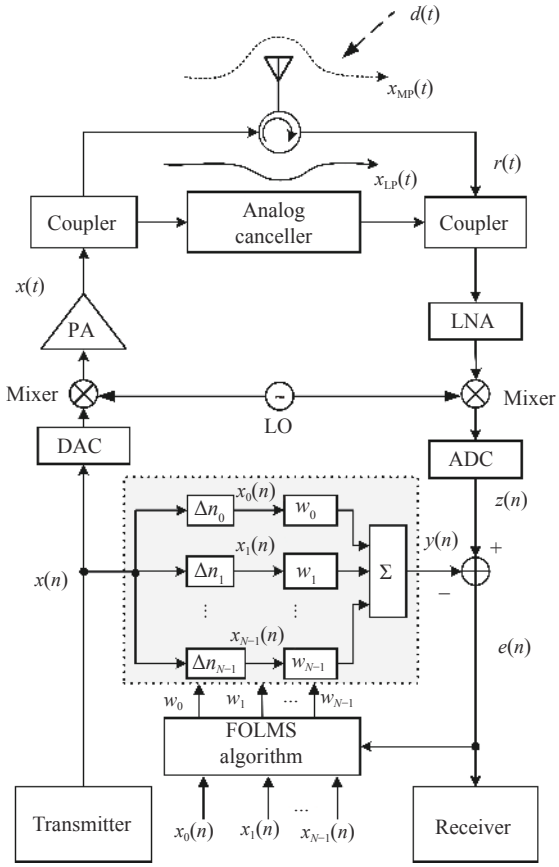

Fig. 1 Block diagram of LFMCW radar with analog domain and digital domain SIC stages

In the model, $x(t)$, $d(t)$ and $r(t)$ are the radar transmitted signal, the echo signal and the received signal, respectively. PA and LNA represent the power amplifier and the low noise amplifier, respectively. $x(t)$ is sent into the circulator and radiated through a single antenna. Because of the lack of the circulator isolation and the space coupling of electromagnetic waves, the receiver channel receives the SI signal from the transmitter. The SI signal $x_{\mathrm{SI}}(t)$ consists of the strong leakage SI signal $x_{\mathrm{LP}}(t)$ and the space multi-path component $x_{\mathrm{MP}}(t)$ [25], which is modeled as $x(t)$ through the Rician fading channel model. In the radar receiver, the SI signal $x_{\mathrm{SI}}(t)$ can be written as

$$x_{\mathrm{SI}}(t)=\sum_{l=0}^{L-1}a_l x(t-\tau_l)=x_{\mathrm{LP}}(t)+x_{\mathrm{MP}}(t) \tag{1}$$

where a_l refers to the amplitude attenuation coefficient and τ_l is time delay in the lth SI signal coupling path. The radio frequency (RF) signal of the radar receiver before cancellation can be expressed as

$$r(t)=d(t)+x_{\mathrm{SI}}(t)+v(t) \tag{2}$$

where $d(t)$ is the echo signal reflected by the target. We assume that it is uncorrelated with transmitted signal $x(t)$.

The noise signal $v(t)$ is a zero-mean Gaussian noise and uncorrelated with $d(t)$ and $x(t)$.

After the ASIC, a multi-path cancellation scheme is shown in Fig. 1 at the digital domain. Each path includes different fixed time delays and the complex weighting coefficient that is controllable by adaptive algorithms. All paths are combined to get the digital reconstructed SI signal $y(n)$, i.e.,

$$y(n)=\sum_{i=0}^{N-1} w_i^*(n)\,x_i(n) \tag{3}$$

where $x_i(n)=x(n-\Delta n_i)$ and i is the index of the path. $w_i(n)$ and $x_i(n)$ are the complex weighting coefficients and the baseband version of the signal $x(t)$ in the ith path, respectively. N is the number of paths and Δn_i is shifted sampling points of the i th path. The N baseband signals are multiplied by the complex weights to adjust the amplitude and phase of the signals, and we combine the N adjusted signals to obtain $y(n)$ at the current time.

Then, the cancellation signal $y(n)$ is subtracted from $z(n)$ to obtain the digital residual signal $e(n)$, i.e.,

$$\begin{aligned} e(n)&=z(n)-y(n)=\\ &x_{re}(n)+d(n)+v(n)-\sum_{i=0}^{N-1} w_i^*(n)\,x_i(n) \end{aligned} \tag{4}$$

where $x_{re}(n)$ is a discrete representation of the analog residual SI signal, $d(n)$ is a discrete representation of the analog echo signal.

In order to adapt to the impact of changes on the SI channel, the complex coefficients must be estimated adaptively and precisely to ensure SI suppression processing. Therefore, the adaptive algorithm is deployed to tune and update the coefficients.

3. ADSIC method

3.1 ADSIC method based on FOLMS algorithm

In the ADSIC method, $J(n)$ is defined as the instantaneous power of the digital residual signal $e(n)$, and can be described as

$$J(n)=|e(n)|^2=e(n)e^*(n) \tag{5}$$

where $|\cdot|$ means the absolute value operation. Ideally, there are only the echo signal and noise in the residual signal $e(n)$ after SIC. Therefore, $J(n)$ is a convex quadric surface with a unique extreme point.

Equation (3) indicates that the crucial parameter to SIC is the complex weighting coefficients $w_i(n)$, which can be determined by minimizing $J(n)$, i.e.,

$$\min_{w_i(n)} J(n)=\min_{w_i(n)} e(n)e^*(n). \tag{6}$$

The LMS-based ADSIC method utilizes the IOGD to update its complex weighting coefficients. The FOLMS-based ADSIC improves the SIC performance by replacing IOGD by FOGD. In this case, the coefficient in the ith channel updating equation is expressed as

$$w_i(n+1)=w_i(n)+\mu\left[-\frac{\partial^\alpha J(n)}{\partial w_i^*(n)^\alpha}\right] \tag{7}$$

where α is the fractional order. $\partial^\alpha J(n)/\partial w_i^*(n)^\alpha$ represents the partial derivative of $J(n)$ for $w_i^*(n)$. For any constant $m-1<\alpha<m$, $m\in\mathbf{N}^+$, Caputo's derivative with order α for a smooth convex function $J(n)$ can be written in a form as the Taylor series [26]:

$${}_{w_i^*(0)}{}^{C}\mathrm{D}^{\alpha}_{w_i^*(n)}J(n)=\sum_{k=m}^{\infty}\frac{J_0^{(k)}(n)}{\Gamma(k+1-\alpha)}\cdot\left[w_i^*(n)-w_i^*(0)\right]^{k-\alpha} \tag{8}$$

where ${}_a^C D_b^\alpha$ denotes the Caputo's fractional differential operator between a and b, and $J_0^{(k)}(n)$ represents the kth order partial derivative of $J(n)$ at $w_i^*(0)$.

The convergence of FOLMS cannot be guaranteed in (8) due to the long memory characteristics of fractional derivative. Therefore, in order to reduce the memory characteristics, the initial integral point $w_i^*(0)$ is replaced with $w_i^*(n-1)$ to update at each step, so (8) is rewritten as

$$\begin{aligned} {}_{w_i^*(n-1)}{}^{C}\mathrm{D}^{\alpha}_{w_i^*(n)}J(n)&=\sum_{k=0}^{\infty}\frac{J_{n-1}^{(k+1)}(n)}{\Gamma(k+2-\alpha)}\cdot\\ &\left[w_i^*(n)-w_i^*(n-1)\right]^{k+1-\alpha} \end{aligned} \tag{9}$$

where the order $0<\alpha<1$ and $J_{n-1}^{(k+1)}(n)$ represents the $(k+1)$th order partial derivative of $J(n)$ at $w_i^*(n-1)$.

Next, the steady state of the algorithm is discussed. $J_{n-1}^{(1)}(n)/\Gamma(2-\alpha)\cdot\left[w_i^*(n)-w_i^*(n-1)\right]^{1-\alpha}$ mainly determines the value of (9) when $|w_i^*(n)-w_i^*(n-1)|\to 0$, so we can only reserve the first item to simplify the equation [26], i.e.,

$${}_{w_i^*(n-1)}{}^{C}\mathrm{D}^{\alpha}_{w_i^*(n)}J(n)=\frac{J_n^{(1)}(n)}{\Gamma(2-\alpha)}\cdot\left[w_i^*(n)-w_i^*(n-1)\right]^{1-\alpha} \tag{10}$$

where $0<\alpha<1$ and $J_n^{(1)}(n)$ represents the first order partial derivative of $J(n)$ at $w_i^*(n)$ to be consistent with (7). Taking (10) into (7), and regarding $\Gamma(2-\alpha)$ as part of μ, we have

$$w_i(n+1)=w_i(n)-\mu J_n^{(1)}(n)\cdot\left[w_i^*(n)-w_i^*(n-1)\right]^{1-\alpha} \tag{11}$$

where $0<\alpha<1$ and $\mu>0$. To keep $\mu\left[w_i^*(n)-w_i^*(n-1)\right]^{1-\alpha}$ be positive all the time and extend α to (1, 2), (11) can be further transformed into

$$w_i(n+1)=w_i(n)-\mu J_n^{(1)}(n)\cdot\left[|w_i(n)-w_i(n-1)|+\delta\right]^{1-\alpha} \tag{12}$$

where $0<\alpha<2$ and $J_n^{(1)}(n)=2\tilde{x}_i(n)e^*(n)$. δ is a small positive scalar, which is to avoid singularity when $1<\alpha<2$. However, δ is 0 when $0<\alpha<1$. From (12), the conventional LMS is the special case of FOLMS with $\alpha=1$.

To be simple, (12) can be written in the vector form as

$$\boldsymbol{W}(n+1)=\boldsymbol{W}(n)+2\mu\Delta\boldsymbol{W}_n^{1-\alpha}\boldsymbol{X}(n)e^*(n) \tag{13}$$

where $\boldsymbol{W}(n)=[w_0(n),\ w_1(n),\ \cdots,\ w_{N-1}(n)]^{\mathrm{T}}$, $\boldsymbol{X}(n)=[x_0(n),\ x_1(n),\ \cdots,\ x_{N-1}(n)]^{\mathrm{T}}$, called the digital baseband reference signal, and the diagonal matrix $\Delta\boldsymbol{W}_n^{1-\alpha}=\mathrm{diag}\{[|w_0(n)-w_0(n-1)|+\delta]^{1-\alpha},\ \cdots,\ [|w_{N-1}(n)-w_{N-1}(n-1)|+\delta]^{1-\alpha}\}$.

3.2 Performance evaluation

In general, the interference cancellation ratio (ICR) is used to evaluate the cancellation performance of the ADSIC method, which can be defined as

$$\mathrm{ICR}=10\lg\frac{P_z-P_d-P_v}{P_e-P_d-P_v} \tag{14}$$

where P_z is the power of the residual signal $z(n)$ before the digital canceller and P_d is the power of echo signal $d(n)$. P_e is the power of the residual signal $e(n)$ after the digital canceller and P_v is the power of noise signal $v(n)$. Obviously, ICR is in an inverse relation with P_e, the smaller P_e, the higher ICR and the better performance of ADSIC.

If the reference signal $\boldsymbol{X}(n)$ is the stationary signal, such as the single tone signal, Wiener solution of the ADSIC system is stable. However, the reference signal is the non-stationary in LFMCW radar. The non-stationary characteristics of the LFM transmitted signal will make the optimal weighting coefficients of taps, $\boldsymbol{W}_{\mathrm{opt}}(n)=[w_{0\mathrm{opt}}(n),\ w_{1\mathrm{opt}}(n),\ \cdots,\ w_{N-1\mathrm{opt}}(n)]^{\mathrm{T}}$, also changes with time. In this case, the SI suppression performance is related to the adaptive adjustment ability of the proposed method closely. Therefore, in the actual LFMCW radar applications, the adaptive algorithm performs an additional task, which is tracking the time-varying position of the minimum value on the cost function performance surface.

In the non-stationary signals, the $\boldsymbol{\varepsilon}(n)$ and $\boldsymbol{Q}(n)$ are defined as

$$\begin{cases}\boldsymbol{\varepsilon}(n)=\boldsymbol{W}(n)-\boldsymbol{W}_{\mathrm{opt}}(n)\\ \boldsymbol{Q}(n+1)=\boldsymbol{W}_{\mathrm{opt}}(n+1)-\boldsymbol{W}_{\mathrm{opt}}(n)\end{cases} \tag{15}$$

where $\boldsymbol{\varepsilon}(n)$ and $\boldsymbol{Q}(n)$ are nonzero in LFMCW radar ADSIC theoretically. Then, the residual SI signal $x_{re}(n)$ after analog canceller is also written as

$$x_{re}(n)=\boldsymbol{W}_{\mathrm{opt}}^{\mathrm{H}}(n)\boldsymbol{X}(n)+e_o(n) \tag{16}$$

where $e_o(n)$ is the evaluated error, which is a white Gaussian noise and mutual statistical independence with the reference signal $\boldsymbol{X}(n)$. By (13), (15) and (16), we can get that

$$\begin{aligned}\mathrm{E}[\boldsymbol{\varepsilon}(n+1)]=\mathrm{E}\big[&\boldsymbol{\varepsilon}(n)-\boldsymbol{Q}(n+1)-\\ &2\mu\Delta\boldsymbol{W}_n^{1-\alpha}\boldsymbol{X}(n)\boldsymbol{X}^{\mathrm{H}}(n)\boldsymbol{\varepsilon}(n)+\\ &2\mu\Delta\boldsymbol{W}_n^{1-\alpha}\boldsymbol{X}(n)e_o^*(n)\big]=\mathrm{E}[\boldsymbol{\varepsilon}(n)]-\mathrm{E}[\boldsymbol{Q}(n+1)]-\\ &2\mu\Delta\boldsymbol{W}_{n,\mathrm{E}}^{1-\alpha}\boldsymbol{R}(n)\mathrm{E}[\boldsymbol{\varepsilon}(n)]\end{aligned} \tag{17}$$

where $\mathrm{E}[2\mu\Delta\boldsymbol{W}_n^{1-\alpha}\boldsymbol{X}(n)e_O^*(n)]=0$, $\Delta\boldsymbol{W}_{n,\mathrm{E}}^{1-\alpha}=\mathrm{E}[\Delta\boldsymbol{W}_n^{1-\alpha}]$ and $\boldsymbol{R}(n)$ is the autocorrelation matrix of the vector $\boldsymbol{X}(n)$. $\boldsymbol{R}(n)$ is the Hermitian matrix, which can be represented as

$$\boldsymbol{R}(n)=\boldsymbol{H}(n)\boldsymbol{\Lambda}(n)\boldsymbol{H}^{\mathrm{H}}(n) \tag{18}$$

where $\boldsymbol{H}(n)$ is the unitary matrix and $\boldsymbol{\Lambda}(n)$ is the diagonal matrix which consists of $\boldsymbol{R}(n)$ eigenvalues. Because $\boldsymbol{R}(n)$ is a positive definite matrix, the diagonal elements of diagonal matrix $\boldsymbol{\Lambda}(n)$ are all positive real numbers. Multiply (17) by $\boldsymbol{H}^{\mathrm{H}}(n)$, which is converted to

$$\begin{aligned}\mathrm{E}\big[\boldsymbol{H}^{\mathrm{H}}(n)\boldsymbol{\varepsilon}(n+1)\big]=&\mathrm{E}\big[\boldsymbol{H}^{\mathrm{H}}(n)\boldsymbol{\varepsilon}(n)\big]-\\ &\mathrm{E}\big[\boldsymbol{H}^{\mathrm{H}}(n)\boldsymbol{Q}(n+1)\big]-2\mu\Delta\boldsymbol{W}_{n,\mathrm{E}}^{1-\alpha}\boldsymbol{\Lambda}(n)\mathrm{E}\big[\boldsymbol{H}^{\mathrm{H}}(n)\boldsymbol{\varepsilon}(n)\big].\end{aligned} \tag{19}$$

When the modulation rate of the LFM signal is small, the statistical characteristics of the signal change slowly. After the algorithm converges to the steady state, the approximation can be obtained.

$$\mathrm{E}[\boldsymbol{H}^{\mathrm{H}}(n)\boldsymbol{\varepsilon}(n+1)]\approx\mathrm{E}[\boldsymbol{H}^{\mathrm{H}}(n+1)\boldsymbol{\varepsilon}(n+1)] \tag{20}$$

According to (20), (19) can be further expressed as

$$\begin{aligned}\mathrm{E}[\boldsymbol{\varepsilon}'(n+1)]=&\mathrm{E}[\boldsymbol{\varepsilon}'(n)]-\mathrm{E}[\boldsymbol{Q}'(n+1)]-\\ &2\mu\Delta\boldsymbol{W}_{n,\mathrm{E}}^{1-\alpha}\boldsymbol{\Lambda}(n)\mathrm{E}[\boldsymbol{\varepsilon}'(n)]\end{aligned} \tag{21}$$

where $\boldsymbol{\varepsilon}'(n+1)=\boldsymbol{H}^{\mathrm{H}}(n+1)\boldsymbol{\varepsilon}(n+1)$, $\boldsymbol{\varepsilon}'(n)=\boldsymbol{H}^{\mathrm{H}}(n)\boldsymbol{\varepsilon}(n)$, $\boldsymbol{Q}'(n+1)=\boldsymbol{H}^{\mathrm{H}}(n)\boldsymbol{Q}(n+1)$.

Mean square deviation (MSD) $D(n)$ and mean square error (MSE) $\xi(n)$ are defined as

$$\begin{cases}D(n)=\mathrm{E}\big[\|\boldsymbol{\varepsilon}(n)\|_2^2\big]\\ \xi(n)=\mathrm{E}\big[\big|\boldsymbol{\varepsilon}^{\mathrm{H}}(n)\boldsymbol{X}(n)\big|^2\big]\end{cases} \tag{22}$$

where $\|\cdot\|_2^2$ is the square of the Euclidean norm. When $W(n)$ is closer to Wiener solution $W_{\mathrm{opt}}(n)$ in the vector space, the MSD and the MSE are smaller.

We write $D(n+1)$ as

$$D(n+1)=\mathrm{E}\left[\|\boldsymbol{\varepsilon}(n+1)\|_2^2\right]=$$
$$\mathrm{E}\left\{\sum_{i=0}^{N-1}\left\{|\varepsilon'_i(n)|^2+\left|q'_i(n+1)\right|^2+\right.\right.$$
$$4\mu^2\left(\Delta w_{in}^{1-\alpha}\right)^2\lambda_i^2(n)|\varepsilon'_i(n)|^2+$$
$$4\mu\Delta w_{in}^{1-\alpha}\lambda_i(n)\cdot\mathrm{Re}\left[\varepsilon'_i(n)q'^{*}_i(n+1)\right]-$$
$$\left.\left.4\mu\Delta w_{in}^{1-\alpha}\lambda_i(n)|\varepsilon'_i(n)|^2-2\mathrm{Re}\left[\varepsilon'_i(n)q'^{*}_i(n+1)\right]\right\}\right\} \quad (23)$$

where $\Delta w_{in}^{1-\alpha}$ is the ith diagonal element of diagonal matrix $\Delta \boldsymbol{W}_n^{1-\alpha}$, and $\lambda_i(n)$ is the ith diagonal element of diagonal matrix $\boldsymbol{\Lambda}(n)$. $\varepsilon'_i(n)$ and $q'_i(n+1)$ are the elements of matrix $\boldsymbol{\varepsilon}(n)$ and $\boldsymbol{Q}(n+1)$, respectively.

In order to analyze the effects of step size μ and fractional order α on MSD, we suppose that

$$S(n)=4\lambda_i^2(n)|\varepsilon'_i(n)|^2\mu_{\mathrm{FO}}{}^2+$$
$$\left\{4\lambda_i(n)\mathrm{Re}\left[\varepsilon'_i(n)q'^{*}_i(n+1)\right]-4\lambda_i(n)|\varepsilon'_i(n)|^2\right\}\mu_{\mathrm{FO}} \quad (24)$$

where μ_{FO} is the equivalent step size of the FOLMS method and $\mu_{\mathrm{FO}}=\mu\Delta w_{in}^{1-\alpha}>0$. The effects of step size and fractional order on MSD can be considered as the effects on function $S(n)$. Function $S(n)$ can be regarded as a quadratic function of variable μ_{FO}. Since the coefficient of the quadratic term, $4\lambda_i^2(n)\left|\varepsilon'_i(n)\right|^2$, is more than 0, the curve of the function is a parabola with opening upwards, and there is a symmetry axis μ_{FO}^*, which is given as

$$\mu_{\mathrm{FO}}^*=-\frac{\mathrm{Re}\left[\varepsilon'_i(n)q'^{*}_i(n+1)\right]-|\varepsilon'_i(n)|^2}{2\lambda_i(n)|\varepsilon'_i(n)|^2}. \quad (25)$$

According to the position of the symmetry axis and the value of μ_{FO}, MSD and MSE can be divided into the following cases:

(i) When the symmetry axis $\mu_{\mathrm{FO}}^*>0$, $S(n)$ is a decreasing function in $0<\mu_{\mathrm{FO}}<\mu_{\mathrm{FO}}^*$ and $S(n)$ is an increasing function in $\mu_{\mathrm{FO}}>\mu_{\mathrm{FO}}^*$. $S(n)$ obtains the minimum value at the symmetrical axis μ_{FO}^*.

i) When $|w_i(n)-w_i(n-1)|<1$ and $\alpha>1$, $\Delta w_{in}^{1-\alpha}>1$, then $\mu_{\mathrm{FO}}=\mu\Delta w_{in}^{1-\alpha}>\mu$. If $0<\mu_{\mathrm{FO}}<\mu_{\mathrm{FO}}^*$, then $S(n)$ of the FOLMS method is less than $kS(n)$ of the LMS method, i.e., $S_{\mathrm{FO}}(n)<S_{\mathrm{LMS}}(n)$, which further leads to that $D(n+1)$ of the FOLMS method is less than $D(n+1)$ of the LMS method, i.e., $D_{\mathrm{FO}}(n+1)<D_{\mathrm{LMS}}(n+1)$ and $\xi(n+1)$ of the FOLMS method is less than $\xi(n+1)$ of the LMS method, i.e., $\xi_{\mathrm{FO}}(n+1)<\xi_{\mathrm{LMS}}(n+1)$. At this point, the ICR of the FOLMS method is higher than that of the LMS method; when $\mu_{\mathrm{FO}}>\mu_{\mathrm{FO}}^*$ and $\mu_{\mathrm{FO}}>\mu$, then $S_{\mathrm{FO}}(n)>S_{\mathrm{LMS}}(n)$. We get $D_{\mathrm{FO}}(n+1)>D_{\mathrm{LMS}}(n+1)$ and $\xi_{\mathrm{FO}}(n+1)>\xi_{\mathrm{LMS}}(n+1)$. Now, the ICR of the LMS method is higher than that of the FOLMS method.

ii) When $|w_i(n)-w_i(n-1)|<1$ and $\alpha<1$, $\Delta w_{in}^{1-\alpha}<1$, then $\mu_{\mathrm{FO}}=\mu\Delta w_{in}^{1-\alpha}<\mu$. If $0<\mu_{\mathrm{FO}}<\mu_{\mathrm{FO}}^*$, then $S_{\mathrm{FO}}(n)>S_{\mathrm{LMS}}(n)$, which further leads to $D_{\mathrm{FO}}(n+1)>D_{\mathrm{LMS}}(n+1)$ and $\xi_{\mathrm{FO}}(n+1)>\xi_{\mathrm{LMS}}(n+1)$. At this time, the ICR of the LMS method is higher than that of the FOLMS method; when $\mu_{\mathrm{FO}}>\mu_{\mathrm{FO}}^*$ and $\mu_{\mathrm{FO}}<\mu$, then $S_{\mathrm{FO}}(n)<S_{\mathrm{LMS}}(n)$. We get $D_{\mathrm{FO}}(n+1)<D_{\mathrm{LMS}}(n+1)$ and $\xi_{\mathrm{FO}}(n+1)<\xi_{\mathrm{LMS}}(n+1)$. Now, the ICR of the FOLMS method is higher than that of the LMS method. In practice, we generally select a smaller step size to ensure the stability of the adaptive algorithm.

(ii) When the symmetry axis $\mu_{\mathrm{FO}}^*<0$, $S(n)$ is a increasing function in the range of $\mu_{\mathrm{FO}}>0$.

i) When $|w_i(n)-w_i(n-1)|<1$ and $\alpha>1$, $\Delta w_{in}^{1-\alpha}>1$, then $\mu_{\mathrm{FO}}>\mu$ and $S_{\mathrm{FO}}(n)>S_{\mathrm{LMS}}(n)$, which further leads to $D_{\mathrm{FO}}(n+1)>D_{\mathrm{LMS}}(n+1)$ and $\xi_{\mathrm{FO}}(n+1)>\xi_{\mathrm{LMS}}(n+1)$. At this time, the ICR of LMS is higher than that of FOLMS.

ii) When $|w_i(n)-w_i(n-1)|<1$ and $\alpha<1$, $\Delta w_{in}^{1-\alpha}<1$, then $\mu_{\mathrm{FO}}<\mu$ and $S_{\mathrm{FO}}(n)<S_{\mathrm{LMS}}(n)$, which further leads to $D_{\mathrm{FO}}(n+1)<D_{\mathrm{LMS}}(n+1)$ and $\xi_{\mathrm{FO}}(n+1)<\xi_{\mathrm{LMS}}(n+1)$. By this time, the ICR of FOLMS is higher than that of LMS.

In LFMCW radar, the modulation rate of $x(n)$ is a significant factor affecting the Wiener solution $\boldsymbol{W}_{\mathrm{opt}}(n)$. The dynamic range of $\boldsymbol{W}_{\mathrm{opt}}(n)$ is proportional to the modulation rate. For LFMCW radar with the large modulation rate, the LMS-based ADSIC method cannot make the change of $\boldsymbol{W}(n)$ match that of $\boldsymbol{W}_{\mathrm{opt}}(n)$ only by adjusting the step size, which leads to the fact that the SI component cannot be fully suppressed. Different from LMS, the proposed algorithm can make $\boldsymbol{W}(n)$ well track $\boldsymbol{W}_{\mathrm{opt}}(n)$ by selecting the appropriate fractional order. From the above analyses in (i) and (ii), the fractional order in FOLMS is usually set to a value greater than 1 to improve the ICR of ADSIC system when the modulation rate of $x(n)$ is large.

Different from LMS, the FOLMS has an extra power term $\Delta \boldsymbol{W}_n^{1-\alpha}$. The existence of this component increases the complexity of the proposed algorithm. In the updating of weight coefficient, only one multiplication, two additions and one power operation are added to the calculation of each order coefficient. In the application that calculation accuracy is not strict, $\Delta \boldsymbol{W}_n^{1-\alpha}$ can be simplified by approximate calculation to reduce the computational complexity of FOLMS.

4. Simulation results

The performance of the FOLMS-based ADSIC method is verified by the experiments on simulation data and measured in Matlab. The nonlinear and ADC quantization noise are not considered for the time being. In the simulations, we take the triangular wave modulated LFM signal as the transmitted signal, which is with a sample rate of 100 MHz and a sweep repetition period of 100 μs. The sweep bandwidth is 20 MHz. The SI channel is modeled

as Rice channel, the number of delay paths is 25, and the delay time satisfies the uniform distribution of the range [0, 10] ns. In the ADSIC structure, the number of paths is N=4. We suppose that the noise level of the receiver channel is −97.8 dBmW, and the SI power is −11.5 dBmW after the SSIC and ASIC.

4.1 Simulation experiments of SI suppressing

4.1.1 SIC performance versus fractional order α

In the digital cancellation stage, we contrast the experimental results between the LMS method and the FOLMS method. The power of the residual signal with different fractional orders are shown in Fig. 2. The results are obtained from 1 000 Monte Carlo simulations. When the order α=1.1, the power of the FOLMS method is lower than the LMS method approximately by 13 dB with the same step size. The level of the residual signal power is closer to the noise floor with the FOLMS method (α=1.1) than the LMS method. However, the LMS method has the lower power level of the residual signal than the FOLMS method with α=0.9.

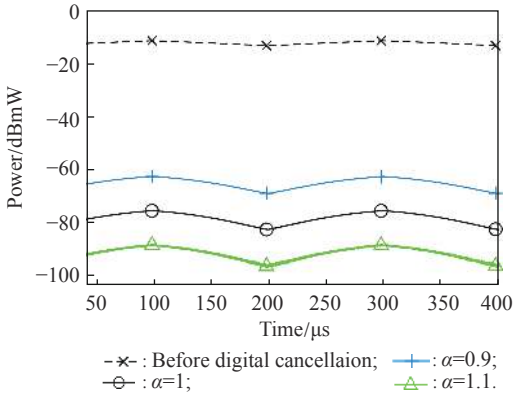

Fig. 2 Power of the residual signal versus various α

In this experiment, $|w_i(n)-w_i(n-1)|<1$, when $1<\alpha\leqslant 1.2$, $|w_i(n)-w_i(n-1)|^{1-\alpha}$ increases as α increases and $\mu_{FO}>\mu$. In Fig. 3, when μ=0.01 and $1<\alpha\leqslant 1.2$, it can be observed that ICR of FOLMS is larger than that of LMS obviously. Then, $\xi(n)$ of the FOLMS method is less than the LMS method, which implies the FOLMS method holds excellent ability of tracking performance. For example, when μ= 0.01 and α=1.1, ICR is 69.4 dB, but LMS is only 56.31 dB. However, it is worth noting that ICR will become diminished when α is greater than a certain range for the same μ. The reason is that when μ_{FO} increases, μ_{FO} will be larger than μ_{FO}^{*} and the iterative search method of the algorithm is changed from the asymptotic way to the oscillatory way, which makes $\xi(n)$ become larger. In other words, the SI suppression performance of the proposed method with α>1 is better than that of LMS when the step size μ is within a reasonable range. Moreover, the proposed method has an optimal fractional order to obtain the highest ICR when μ is fixed, and the optimal fractional order decreases with the increase of μ.

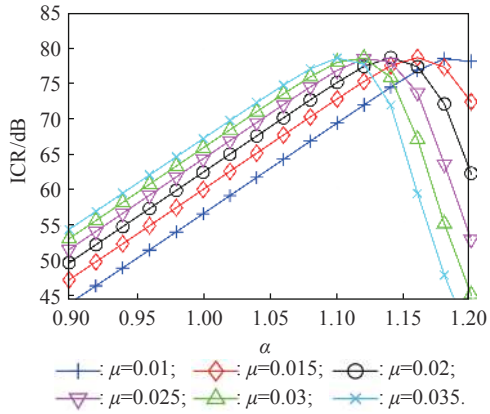

Fig. 3 ICR versus α under various μ

In terms of the power spectral density (PSD), Fig. 4 indicates that if the fractional order α>1, then the SI signal can be cancelled more efficiently in the FOLMS algorithm than the LMS algorithm.

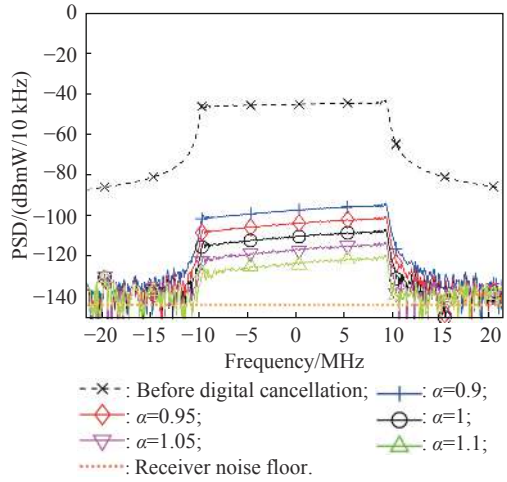

Fig. 4 PSD of the residual signal versus various α

The power of different residual signals is shown in Table 1. Before ADSIC, the power of the received signal is −11.5 dBmW. As μ= 0.03 and α=1, the power of residual signal $e(n)$ is −77.16 dBmW. LMS can suppress the SI signal by 65.7 dB. However, at the same step size, if α= 1.1, then the power of residual signal $e(n)$ is −88.94 dBmW. The ICR is in the order of 77 dB compared to the LMS method, the ICR is in the order of 77 dB. Compared to the LMS method, the ICR is improved by about 11 dB in the FOLMS method.

Table 1 Power of the residual signal with different fractional orders

Item	Power/dBmW
Before digital cancellation	−11.50
$\alpha = 0.9$	−64.11
$\alpha = 0.95$	−70.64
$\alpha = 1.00$	−77.16
$\alpha = 1.05$	−83.54
$\alpha = 1.10$	−88.94
Receiver noise floor	−97.80

4.1.2 SIC performance versus bandwidth and INR

In addition, the performance of the digital SI canceller is affected by the signal sweeping frequency rate. If the bandwidth of the LFM signal becomes larger, the sweeping rate will increase when the modulation period is fixed. ICR with different bandwidths is depicted in Fig. 5.

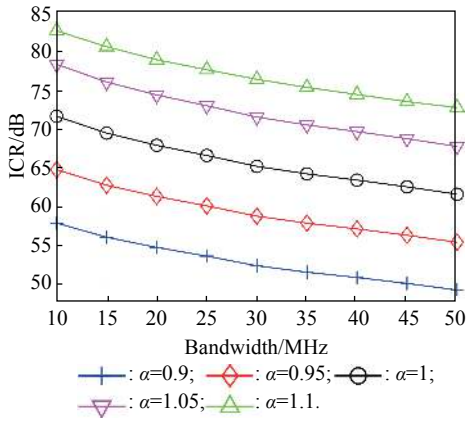

Fig. 5 ICR versus the bandwidth under various α

When α=1.1, the highest ICR value is obtained under the current bandwidth. From the figure, the increasing of the bandwidth, i.e., the increasing of the sweeping rate, will cause ICR to decrease. It means that if the sweeping rate is increasing, then the change of the complex coefficients is not able to adapt the variation tendency of Wiener resolution. That will make the MSE $\xi(n)$ increase, so ICR will be decreasing. At the same bandwidth, μ_{FO} is increasing with the increasing of α, then E[$J(n)$] is decreasing and ICR is becoming higher. In the wider bandwidth, when simulating, taking $1<\alpha\leqslant 1.1$, ICR of the FOLMS method is also better than LMS at the same step size, which means that the FOLMS-based ADSCI method with the larger fractional order may get higher ICR for LFMCW radar with the larger modulation rate of $x(n)$.

Fig. 6 depicts the impact of the interference-to-noise ratio (INR) on the ADSIC ability. The selection of the step size is the optimal step size of the order α=1.1 in each INR. These curves show that ICR is directly proportional to INR and the proposed method with α>1 is better than the LMS method in all the INR regions. Fig. 6 shows that compared with LMS, the SI suppression performance of the FOLMS method is not obvious under the condition of low INR. However, the FOLMS method is going to surpass the LMS method more and more for α=1.1 with INR increasing. In addition, compared with the LMS method, it overcomes the serious deterioration of ICR under the lower INR. It is noted that when INR is between 10 dB and 40 dB, ICR of the order α=1.05 is close to α=1.1, because the residual signal powers are all particularly close to the noise floor in the cases.

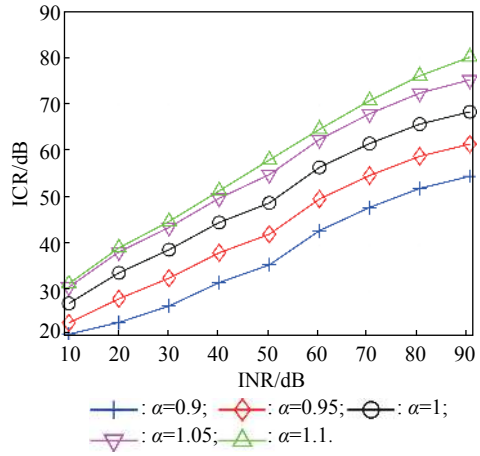

Fig. 6 ICR versus INR under various α

4.1.3 SIC result by the proposed method in actual LFMCW radar

In order to describe the effectiveness of the method further, FOLMS is employed in the actual radar data, which is with a sample rate of 90 MHz and bandwidth of 10 MHz and the sweep repetition period is 90 μs. The power of residual signal $e(n)$ is shown in Fig. 7. When α=1.1, The power of the residual signal obtained by FOLMS is about 7 dB lower than that obtained by LMS. In this case, the FOLMS method obtains about 44 dB SIC.

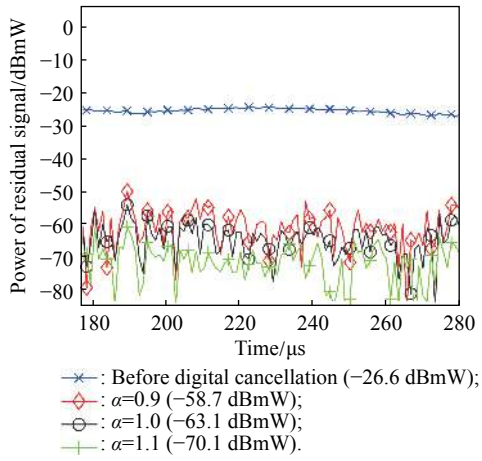

Fig. 7 Power of residual signal versus various α in the actual LFMCW radar

Fig. 8 shows the residual signal PSD under different α cases. It is easy to get that the SI signal in the received signal is suppressed adequately in the frequency bandwidth, and the performance of the FOLMS method with α=1.1 is better than the LMS method. The simulation results demonstrate that FOLMS-based ADSIC is efficient in the actual LFMCW radar.

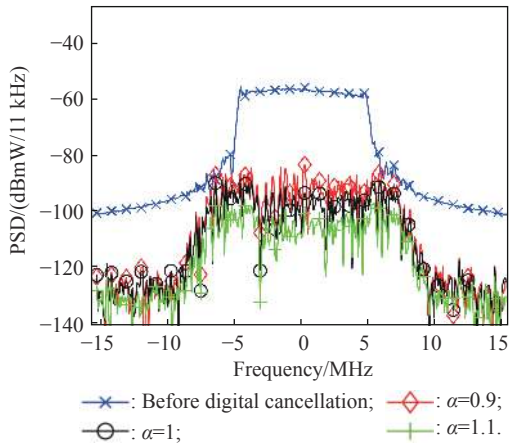

Fig. 8 PSD of the residual signal versus various α in actual LFMCW radar

4.2 Target echo loss effect by the proposed method

In the LFMCW radar, the echo signal is considered in the ADSIC. The radar receiver starts receiving the echo signal after delaying 30 μs, which is reflected from the stationary target, so the Doppler shift is zero. The simulation results are shown in Fig. 9 and Table 2. The echo signal-to-interference signal ratio is defined as the ratio of the beat signal power at 6 MHz to the beat power at 0 MHz.

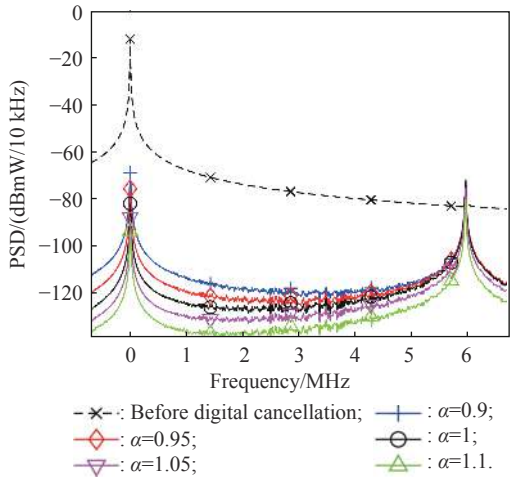

Fig. 9 PSD of the residual signal versus various α after de-chirping

Table 2 PSD and ESIR of the signal with different fractional orders

Item	PSD/(dBmW/10 kHz)		ESIR/dB
	Signal 1	Signal 2	
Before digital cancellation	−12	−71	−59
α = 0.90	−68.5	−71	3.2
α = 0.95	−75.4	−71.7	3.7
α = 1.00	−81.6	−71.7	9.1
α = 1.05	−87.3	−72.5	12.3
α = 1.10	−93.3	−80.1	13.2

In Table 2, signal 1 and signal 2 represent the echo signal and the interference signal after de-chirping, respectively. Before the ADSIC, the PSD of the received signal is −12 dBmW/10 kHz after de-chirping. After the ADSIC, PSD of the residual signal drops to −81.6 dBmW/10 kHz by employing the LMS method. However, the FOLMS method cancels the signal to −93.3 dBmW/10 kHz. The beat signal is at 6 MHz and its level is −71 dBmW/10 kHz before ADSIC, but PSD drops to −72.5 dBmW/10 kHz by the LMS method and −80.1 dBmW/10 kHz by the FOLMS method. From Table 2, when α=1.1, the power of the beat signal 6 MHz is higher than that of the SI signal by approximately 13.2 dB, which is larger than 9.1 dB in the LMS method. The FOLMS method not only eliminates the SI signal adequately, but also makes the beat signal easier to detect. According to Table 2, the ESIR is increasing with the fractional order raising.

To illustrate whether the SIC has an influence on the echo signal, the echo signal cancellation ratio (ESCR) is shown in Fig. 10.

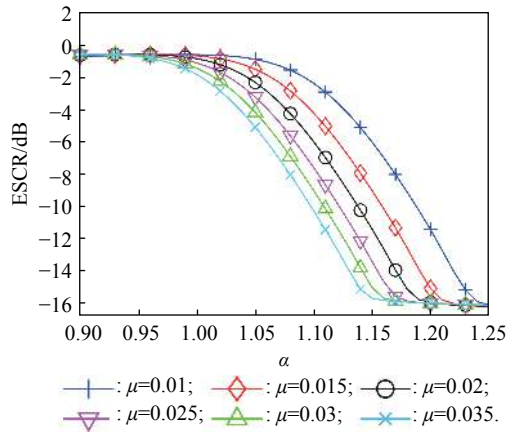

Fig. 10 ESCR of the echo signal versus the fractional order α under various μ

ESCR is given as

$$\mathrm{ESCR} = 10\lg\frac{P_{ae}}{P_{be}} \tag{26}$$

where P_{ae} is the power of the residual echo signal after

the digital canceller and P_{be} is the power of the echo signal before the digital canceller. It is worth noting that the echo signal may be mistaken for the SI signal, so the echo signal will be lost after being processed by the FOLMS or the LMS method. The reasons are that the ADSIC method is based on the LMS criterion, and the cross-correlation function between the echo signal and the reference signal is nonzero in the finite time, which influences the complex coefficients in iteration.

The larger the absolute value of ESCR, the greater the loss of the echo signal. The ESCR of both methods degrades with the increase of the fractional order and the step size, and approaches a value eventually with the larger order. We must eliminate the SI signal and protect the echo signal, so choose the appropriate order and the step size to handle the conflict between them.

4.3 Performance comparison among FOLMS and others methods

We will compare the proposed method with the method in [24] and the conventional LMS-based method. The FOLMS algorithm of [24] is used in the ADSIC model. In order to distinguish it from the method that we proposed, we named it I-FOLMS, which can be written in the vector form as

$$\boldsymbol{W}(n+1)=\boldsymbol{W}(n)+\mu[\boldsymbol{I}(n)+\boldsymbol{T}(n)]\boldsymbol{X}(n)e^{*}(n) \tag{27}$$

where $\boldsymbol{T}(n)$=diag$\{|w_0(n)|^{1-f}, \cdots, |w_{N-1}(n)|^{1-f}\}$, $\boldsymbol{I}(n)$ is the N dimension unit matrix and the fractional order $0<f\leqslant 1$. When $f=1$, it is regarded as the LMS algorithm. Equation (27) can be seen as an IOGD method with an extra fractional order item $\boldsymbol{T}(n)$ added. As $0<f<1$, if $|w_i(n)|>1$, then the value of $|w_i(n)|^{1-f}$ will be larger than 1 that will decrease as the order f increases. Then, $\mu|w_i(n)|^{1-f}>\mu$, the algorithm will obtain a faster convergence rate. On the contrary, $|w_i(n)|^{1-f}$ will be less than 1 when $|w_i(n)|<1$ and it is proportional to the order f. Then, $\mu|w_i(n)|^{1-f}$ will be less than μ, and the smaller steady error will be achieved.

Taking $f\in[0.7, 1.0]$, Fig. 11 shows ICR of the different cases. As for the I-FOLMS method, ICR is increasing with the fractional order f increasing when $\mu\leqslant 0.15$. It is because that when $|w_i(n)|<1$, $\mu|w_i(n)|^{1-f}$ is proportional to the order f. When E[$J(n)$] becomes smaller, ICR is improved. With a step size $\mu=0.2$ and $f>0.9$, ICR decreases as f increases. As mentioned in Fig. 3, the optimal f also exists in the I-FOLMS method. Compared with Fig. 3, the highest ICR of the proposed method and the I-FOLMS method are the same. The reason is that both the proposed method and the I-FOLMS method can make it converge to the extreme point ultimately.

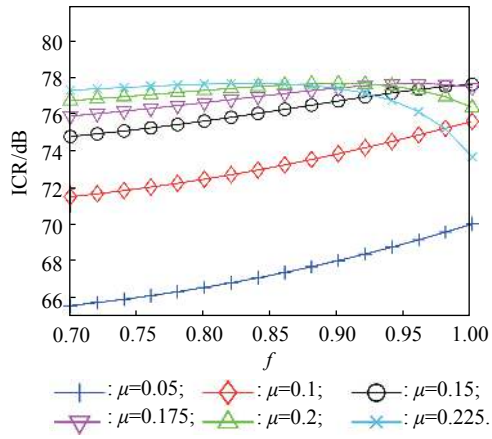

Fig. 11 ICR versus f under various μ

Taking $\mu=0.03$, PSD of the I-FOLMS method and the proposed method are shown in Fig. 12. When $\alpha<1$, PSD of the I-FOLMS method is lower than the proposed method, which means the residual signal power is smaller. In this case, the equivalent step size of the I-FOLMS method is larger than the proposed method μ_{FO}, so the tracking performance of the I-FOLMS method is better. However, the I-FOLMS method obtains the best performance when $f=1$, and PSD of the I-FOLMS method will be higher than the proposed method when $\alpha>1$.

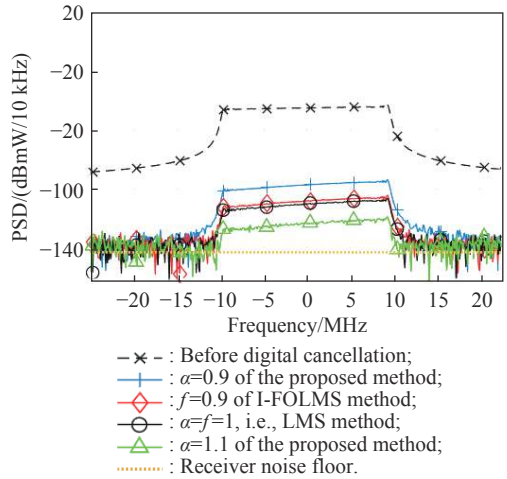

Fig. 12 PSD of different methods versus various fractional orders

5. Conclusions

In this paper, we propose a FOLMS-based ADSIC method in the LFMCW radar. With advantages of the FOGD, the FOLMS method can track the changes of Wiener solution more efficiently than the LMS method. Furthermore, the simulation results of actual LFMCW radar data show that the proposed method is efficacious in the radar. Whether the LMS or the FOLMS is used, the target echo signal will be affected by the SI signal, but the SI sup-

pression effect of the FOLMS is better than that of the LMS. It reduces the adverse effect of SI on the target echo signal detection and makes the target detection more accurate.

References

[1] ARISES H, PRISTIANTO E J, RAHMAN A N, et al. Compact FMCW radar system for navigation application: transmitter front-end design. Proc. of the International Conference on Radar, Antenna, Microwave, Electronics, and Telecommunications, 2017: 6−10.

[2] KIM E H, KIM K H. Random phase code for automotive MIMO radars using combined frequency shift keying-linear FMCW waveform. IET Radar, Sonar and Navigation, 2018, 12(10): 1090–1095.

[3] KIM J, KIM S, LEE S, et al. Vehicle black box with 24GHz FMCW radar. Proc of the IEEE Region 10 Conference, 2016: 1392−1396.

[4] KREJCI T, MANDLIK M. Close vehicle warning for bicyclists based on FMCW radar. Proc. of the 27th International Conference on Radio Electronics, 2017: 1−5.

[5] NARBUDOWICZ A, RUVIO G. Passive self-interference suppression for single-channel full-duplex operation. IEEE Wireless Communications, 2018, 25(5): 64–69.

[6] KORPI D, HEINO M, ICHEIN C, et al. Compact inband full-duplex relays with beyond 100 dB self-interference suppression: enabling techniques and field measurements. IEEE Trans. on Antennas and Propagation, 2016, 65(2): 960–965.

[7] KHALEDIAN S, FARZAMI F, SMIDA B, et al. Robust self-interference cancellation for microstrip antennas by means of phase reconfigurable coupler. IEEE Trans. on Antennas and Propagation, 2018, 66(10): 5574–5579.

[8] EVERETT E, SAHAI A, SABHARWAL A. Passive self-interference suppression for full-duplex infrastructure nodes. IEEE Trans. on Wireless Communications, 2014, 13(2): 680–694.

[9] LU H, HUAMG C, TARANETZ M, et al. Quadrature down conversion based analog self-interference cancellation for continuous wave radars. Proc. of the IEEE Globecom Workshops, 2016: 1−6.

[10] KOLODZIEJ K E, MCMICHAEL J G, PERRY B T. Multitap RF canceller for in-band full-duplex wireless communications. IEEE Trans. on Wireless Communications, 2016, 15(6): 4321–4334.

[11] WANG J, ZHAO H Z, QIN C J, et al. Adaptive self-interference cancellation at RF domain in co-frequency co-time full-duplex systems. Journal of Electronics Information Technology, 2014, 36(6): 1435–1440.

[12] TAMMINEN J, TURUNEN M, KORPI D, et al. Digitally-controlled RF self-interference canceller for full-duplex radios. Proc. of the 24th European Signal Conference, 2016: 783−787.

[13] DEBAILLIE B, VAN DEN BROEK D, LAVIN C, et al. Analog/RF solutions enabling compact full-duplex radios. IEEE Journal on Selected Areas in Communications, 2014, 32(9): 1662–1673.

[14] WANG Q, XU X X. An isolation improvement method for frequency modulated continuous wave radar. Shipboard Electronic Countermeasure, 2018, 41(4): 31–35. (in Chinese)

[15] QI Q, HU H C, WANG D H, et al. Research on digital cancellation technology in FMCW radar. Radar & ECM, 2019, 39(3): 1–4. (in Chinese)

[16] AHMED E, ELTAWIL A M. All-digital self-interference cancellation technique for full-duplex systems. IEEE Trans. on Wireless Communications, 2015, 14(7): 3519–3532.

[17] LI C X, ZHAO H Z, WU F, et al. Digital self-interference cancellation with variable fractional delay fir filter for full-duplex radios. IEEE Communications Letters, 2018, 22(5): 1082–1085.

[18] KOMATSU K, MIYAJI Y, UEHARA H. Basis function selection of frequency domain Hammerstein self-interference canceller for in-band full-duplex wireless communications. IEEE Trans. on Wireless Communications, 2018, 17(6): 3768–3780.

[19] LI N, ZHU W H, HAN H H. Digital interference cancellation in single channel, full duplex wireless communication. Proc. of the 8th International Conference on Wireless Communications, Networking and Mobile Computing, 2012: 1−4.

[20] KRIER J R, AKYILDIZ I F. Active self-interference cancellation of passband signals using gradient descent. Proc. of the IEEE 24th Annual International Symposium on Personal, Indoor, and Mobile Radio Communications, 2013: 1212−1216.

[21] ASHARIF F, TAMAKI S, ALSHARIF M R, et al. Application of full-duplex wireless communication system on echo cancellation. Proc. of the IEEE Wireless Communications and Networking Conference, 2013: 3626−3631.

[22] CHENG S S, WEI Y H, CHEN Y Q, et al. An innovative fractional order LMS based on variable initial value and gradient order. Signal Processing, 2017, 133: 260−269.

[23] ZUBAIR S, CHAUDHARY N I, KHAN Z A, et al. Momentum fractional LMS for power signal parameter estimation. Signal Processing, 2018, 142: 441−449.

[24] RAJA M A Z, QURESHI I M. A modified least mean square algorithm using fractional derivative and its application to system identification. European Journal of Scientific Research, 2009, 35(1): 14–21.

[25] QUAN X, LIU Y, PAN W S, et al. A two-stage analog cancellation architecture for self-interference suppression in full-duplex communications. Proc. of the IEEE MTT-S International Microwave Symposium, 2017: 1169−1172.

[26] CHEN Y Q, GAO Q, WEI Y H, et al. Study on fractional order gradient methods. Applied Mathematics and Computation, 2017, 314: 310–321.

Biographies

LUO Yongjiang was born in 1979. He received his Ph.D. degree in electronic science and technology from Xidian University, Xi'an, China in 2011. He is currently an associate professor in electronic science and technology, Xidian University. His current interests include wideband signal processing, intelligent information processing, fractional systems and signal processing.

E-mail: yjluo@mail.xidian.edu.cn

BI Luhao was born in 1995. He received his B.S. degree in electronic information science and technology from Qingdao University of Technology, Qingdao, China in 2017. He received his M.S. degree in the School of Electronic Engineering, Xidian University, Xi'an, China in 2020. His research interest is radar signal processing.
E-mail: bluhao@163.com

ZHAO Dong was born in 1996. He received his B.S. degree in electronic science and technology from Xi'an University of Posts & Telecommunications, Xi'an, China in 2019. He is currently pursing his M.S. degree in the School of Electronic Engineering, Xidian University, Xi'an, China. His research interest is fractional signal processing.
E-mail: zhaod923@163.com